Int. J. Electrochem. Sci., 8 **(2013)** 7284 - 7297

International Journal of
ELECTROCHEMICAL
SCIENCE
www.electrochemsci.org

Effect of Particle Size on the Photocatalytic Activity and Sensing Properties of CeO_2 Nanoparticles

Sher Bahadar Khan[1,2,*], *M. Faisal*[3], *Mohammed M. Rahman*[1,2], *Kalsoom Akhtar*[4], *Abdullah M. Asiri*[1,2], *Anish Khan*[1,2], *Khalid A. Alamry*[2]

[1] Center of Excellence for Advanced Materials Research (CEAMR), King Abdulaziz University, Jeddah 21589, P.O. Box 80203, Saudi Arabia
[2] Chemistry Department, Faculty of Science, King Abdulaziz University, Jeddah 21589, P.O. Box 80203, Saudi Arabia
[3]Advanced Materials and Nano Research Centre and Department of Chemistry, Faculty of Science and Arts, Najran University, P.O. Box 1988, Najran, 11001, Saudi Arabia
[4] Division of Nano Sciences and Department of Chemistry, Ewha Womans University, Seoul 120-750, Korea
[*]E-mail: sbkhan@kau.edu.sa

Received: 4 November 2012 / *Accepted:* 29 November 2012 / *Published:* 1 May 2013

Cerium oxide (CeO_2 **1**) nanoparticles (NP) have been synthesized hydrothermally in the presence of urea and studied the effect of particle size on the chemical sensing and photo-catalytic properties of CeO_2. CeO_2 **1** was described by field emission scanning electron microscopy (FESEM), Energy dispersive spectroscopy (EDS), X-ray powder diffraction (XRD), Raman spectrum, Fourier transform infrared spectroscopy (FTIR), and UV-visible absorption spectrum which divulged that the prepared product is well crystalline cubic phase optically active nanoparticles. SEM images of CeO_2 **1** illustrated that the synthesized product is composed of cumulative form of highly crytallinity spherical shape nanoparticles with an average diameter of ~ 12 ± 10 nm. Additionally, CeO_2 **1** was exploited as redox mediator for the development of ethanol chemi-sensor. The fabricated chemical sensor exhibited an excellent performance for electrocatalytic oxidization of ethanol by exhibiting higher sensitivity (1.192 $\mu A.cm^{-2}.M^{-1}$) and lower limit of detection (9.7 μM) with the linear dynamic range of 17.0 μM ~ 1.7 M. Moreover, by applying to organic pollutant, CeO_2 **1** degraded almost 50% of acridine orange in short time. By comparing with **2**, CeO_2 **1** showed lower particle size, lower limit of detection and higher sensitivity toward ethanol sensing and high photo-catalytic activity for degradation of acridine orange. It is concluded that reduction in the particle size enhances the active surface area of the CeO_2 which results in increase of chemical sensing and photo-catalytic properties of CeO_2.

Keywords: CeO_2 nanoparticles; Urea; Structural properties; Optical properties; Ethanol chemi-sensor; Photo-catalyst

1. INTRODUCTION

Environmental pollution has received considerable attention due to their harmful effect on human health and living organisms [1-5]. The industrial progress causes several severe environmental problems by releasing wide range of toxic compound to the environment [6,7]. Scrutinizing and investigation of these toxic materials in the environment is important from pollution controlling point of view. Ethanol and dyes are hazardous and toxic pollutants commonly available in the environment due to their continuous release from industries. Ethanol and dye has adverse effect on living organisms [8-10]. They are carcinogenic, hazardous, mutagenic, and toxic (cytotoxic and embryo-toxic) to mammals and badly effect the environment, human health and aquatic ecosystem. [11-14]. Ethanol and dyes have been found in freshwater, marine environments and has been detected in industrial wastewaters because of its high solubility and stability in water. Therefore, it is urgent to build up simple, reliable, easy and efficient technique for detecting of ethanol in aqueous solutions to check and protect water resources and food supplies. Similarly dyes are also risky and unsafe for human health and environment. Thus, it is straight away desirable to develop a photo-catalyst with high degradation activity for the removal of organic pollutants [15-17].

The detection and monitoring of ethanol and degradation of organic pollutants are crucial for environmental pollution control and industrial applications. Various chromatographic and spectroscopic techniques were used for the detection of hazardous solvents but the complication and sluggishness of these techniques affect their importance and vast applications. Electrochemical sensors have gained great attention in the detection and determination of risky compounds because of their simple and fast operation, response and detection [18]. Sensor technology and photo-catalysis plays an important role in environmental safety that normally caused by fortuitous outflow of hazardous chemicals which is a big threat for environment. Thus it is urgent to fabricate simple low cost sensor and active photo-catalyst for the curiosity of environmental and human health. The sensitivity and selectivity of electrochemical sensor strongly dependent on the size, structure and properties of electrode materials and thus semiconductor nanostructured materials have received much importance and has widely been used as a redox mediator in chemical sensors and photo-catalysis [19,20].

Nanomaterials have created a center of attention owing to their distinctive properties and distinguishing performance in various fields especially concern about human health and environmental relevance [15-17]. There are sensible scenario of significant benefits to medicine, environment and energy efficiency. These extensive applications of nanomaterials are mainly considered due to their particular shape, small size, high active surface to volume ratio, and high surface activity. These properties make nanomaterials attractive in many fields. Now a day's nanomaterials have large contribution in sensor technology and photo-catalysis because they are capable to investigate sensing analytes and can degrade organic pollutants. Therefore nanomaterials have enthralled wide attention of the scientific community for their use in the chemical sensor fabrication and photo-catalysis [16-19].

Cerium oxide with different valence states and various crystalline structures have been explored for various applications such as electrical, electronic, catalytic, adsorption, optical, electrochemical, batteries, functional materials, energy storage, magnetic data storage and sensing properties [9,21-24]. However, to enhance various properties of nanomaterials to meet the increasing

needs for different applications, it is needed to reduce the particle size and increase the active surface area of nanomaterials. Decrease in the particle size enhancing conductivity, electrical, sensing and catalytic properties of nonmaterial [25-27]. We have recently synthesized cerium oxide (CeO_2 **2**) by simple hydrothermal reaction and found that it displayed photo-catalytic activity as well as ethanol chemical sensing [22]. We had concluded that cerium oxide could be better candidate as a photo-catalyst and ethanol chemical sensor. However, the photo-catalytic activity and ethanol sensitivity was quite low. To examine our previous conclusion and to improve both the properties, we have extended photo-catalyst and ethanol chemical sensor study to CeO_2 **1** synthesized in the presence of urea.

The aim of this study was to synthesize cerium oxide of low dimension and to explore their properties in chemical sensor and photo-catalytic application. In this paper, a new and sensitive electrochemical sensor has been developed for the detection of ethanol by utilizing newly synthesized cerium oxide (CeO_2 **1**). To widen the application of this new material, CeO_2 **1** is also tasted as a photo-catalyst for the degradation of acridine orange. The newly synthesized nanoparticles exhibited high sensitivity and photo-catalytic activity which can open a new gateway as sensor and photo-catalyst.

2. EXPERIMENTAL DETAILS

2.1. Synthesis of CeO_2 1 nanoparticles

In the synthetic process of CeO_2 **1**, $CeCl_2$ and urea (1:1 molar ratio) were dissolved in distilled water and the pH was raised above 10 by addition of NaOH. The solution was then heated at 150 ºC for 15 hrs in a Teflon-lined autoclave. The obtained product was washed, dried and further calcined calcined at 250 ^{0}C for 5 hours. CeO_2 **2** was also synthesized by the same procedure without urea. The characterization techniques, fabrication of ethanol chemical sensor and photocatalytic degradation procedures of CeO_2 **1** were similar to CeO_2 **2** published elsewhere [22].

3. RESULTS AND DISCUSSION

3.1. Structural and optical properties of synthesized CeO_2 nanoparticles

The morphology and size of the synthesized product (CeO_2 **1)** was described by FESEM images which are shown in Fig. 1. In FESEM, electrons of high energy which is generated by the electron gun hit the sample and thus produce huge number of signal by interaction with the atoms of the sample. These singles are detected by the detector which gives image and information about the surface morphology, features, texture, composition, and crystallographic information of the sample. Thus FESEM is an electron microscope that images a sample by scanning it with a high-energy beam of electrons in a raster scan pattern. Low and high magnification images of FESEM showed that the synthesized product is grown with high density and is composed of cumulative form of spherical shape nanoparticles with an average diameter of ~ 12 ± 10 nm. By comparing with CeO_2 **2**, it was found that CeO_2 **1** has lower particle size which is almost two times smaller than CeO_2 **2** [22]. To assess the

composition of CeO_2 **1**, EDS spectrum was scrutinized and the information is represented in Fig. 2 (a). EDS illustrates peaks linked only to cerium and oxygen like CeO_2 **2** [22] devoid of any impurity peak which verify that produced nanoparticles are made up of cerium and oxygen. Additionally, the atomic percentage of cerium and oxygen was set up to be 32.7 and 67.1 %, correspondingly.

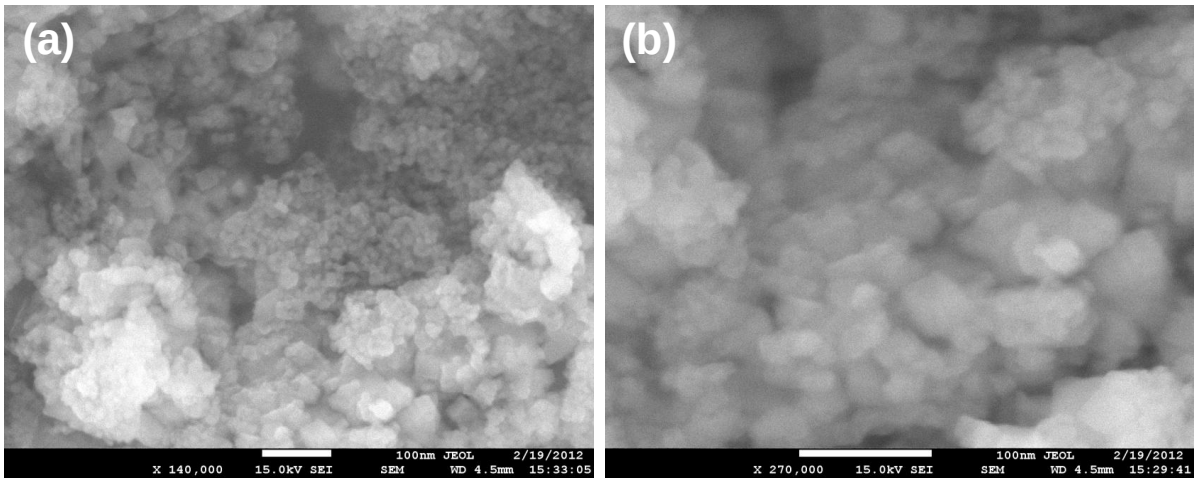

Figure 1. Typical (a) low-magnification and (b) high-resolution FESEM images of CeO_2 **1** nanoparticles.

Crystallinity of the produced nanoparticles was confirmed by XRD which is revealed in Fig. 2 (b). The crystal structure and crystallinity of nano-material is very important characteristic because it eventually affects many physical properties. XRD gives information about the crystal structures and identifying phase of the materials, atomic spacing and unit cell dimensions of crystalline material. The general feature of this XRD patterns in particular the presence of strong and sharp peaks and the absence of diffraction halo, point out that the produced nanoparticles are fine crystalline devoid of amorphous or crystalline-amorphous phase. XRD displayed sharp peaks which situated at 2θ = 28.5, 33.1, 47.5, 56.3, 59.1, 69.4, 76.7, and 79.1 are corresponding to (111), (200), (220), (311), (222), (400), (331), and (420) planes, respectively. The obtained values of d-spacing are in good agreement with that of CeO_2 **2** confirming that CeO_2 **1** has face centered cubic phase (JCPDF cards no 75-8371) [22-24]. According to the PDF cards, the lattice parameter *a* for CeO_2 **1** is 5.4116 Å. All the obtained peaks are more intense and sharp than those of CeO_2 **2** which indicate that CeO_2 **1** is more crystalline than CeO_2 **2** [22]. No other peak associated to impurities was noticed which support that the synthesized nanoparticles are pure CeO_2 with cubic phase [22-24]. The particle size was also calculated and verified using Scherrer formula.

$$D = 0.9\lambda/\beta\cos\theta$$

Where λ is the wavelength of X-ray radiation, β is the full width at half maximum (FWHM) of the peaks. The average diameter of CeO_2 **1** was found to be 12.0 nm.

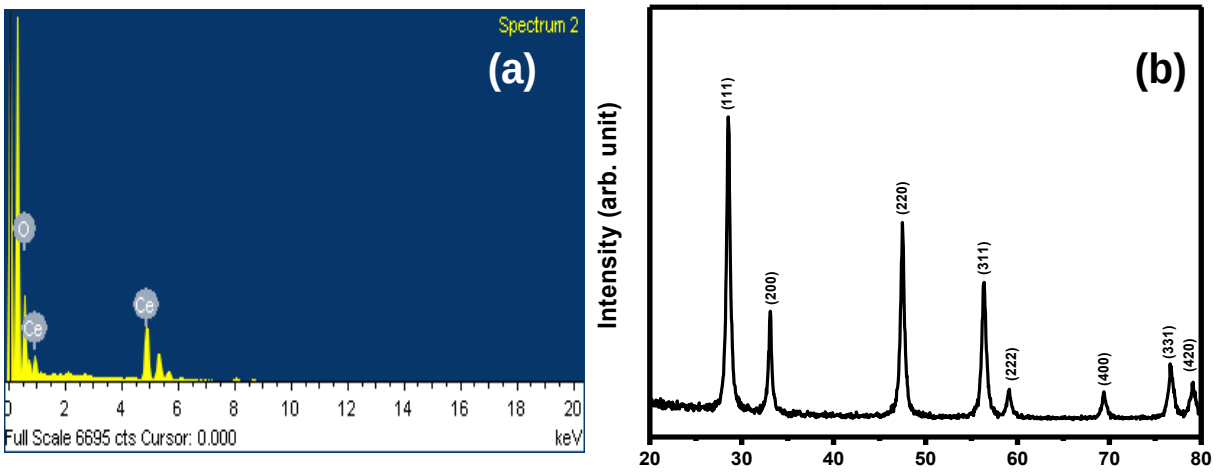

Figure 2. Typical (a) EDS spectrum and (b) XRD pattern of CeO_2 **1** nanoparticles.

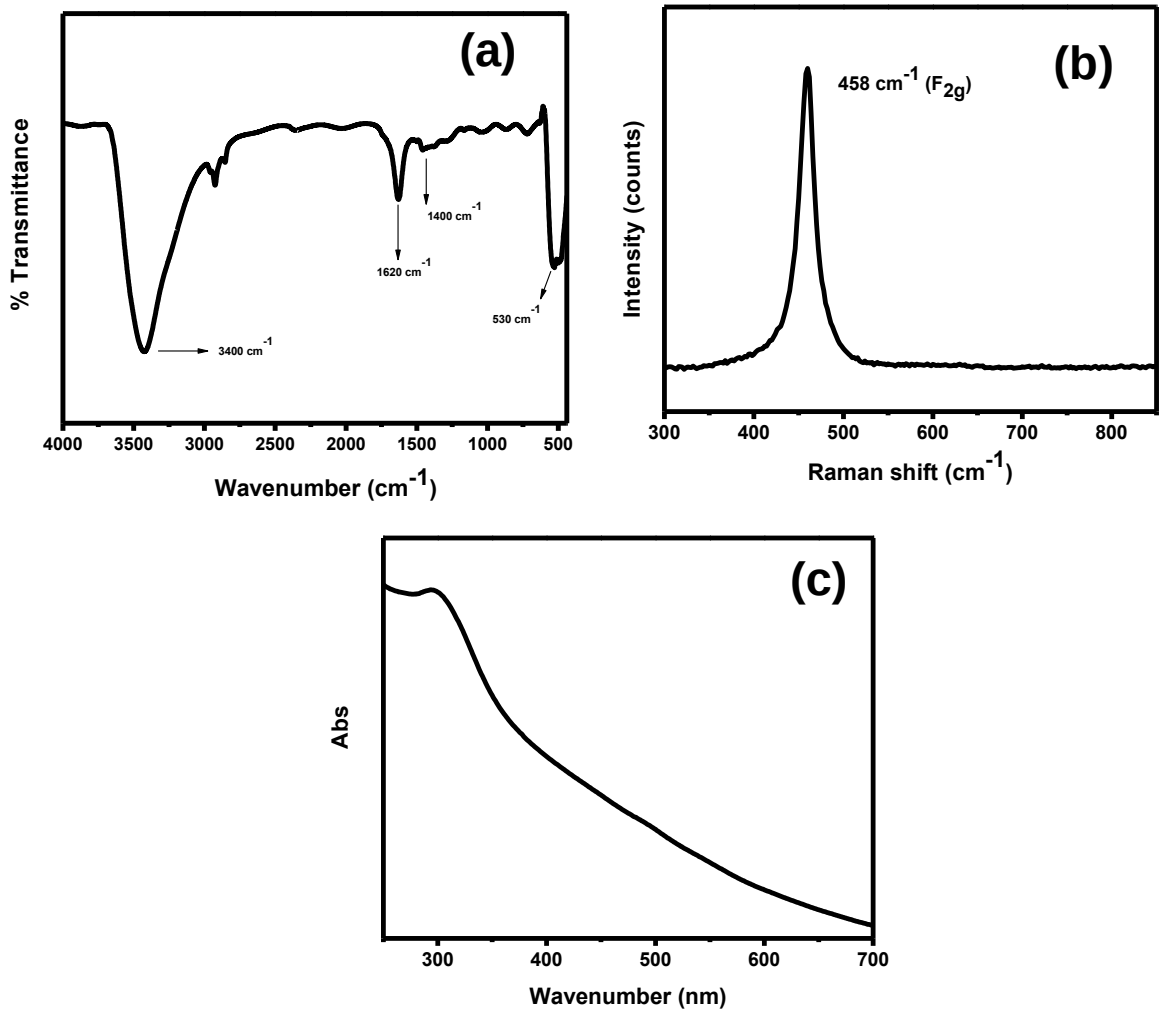

Figure 3. Typical (a) FT-IR spectrum, (b) Raman spectrum and (c) UV-Vis. spectrum of CeO_2 **1** nanoparticles.

The chemical texture of CeO_2 **1** was verified by FT-IR spectrum which is revealed in Fig. 3 (a). FT-IR spectroscopy is a non-destructive method which provides a fingerprint of a sample with absorption peaks which match the frequencies of vibrations among the bonds of material. Different materials have different combination of atoms and thus results in different infrared spectrum. Additionally, the intensity of the peaks in FTIR spectrum provides the information about the magnitude of material. FT-IR illustrated absorption band precisely similar as that of CeO_2 **2** which emerged at 554 cm^{-1} which is the typical peak for the Ce-O stretching vibration [22-24]. FT-IR also exhibited absorption bands at 3343 cm^{-1}, 1600 cm^{-1}, and 1400 cm^{-1} accountable for water and CO_2 which usually nanocrystalline materials take up from the environment due to its high surface-to-volume ratio[22-24]. The FTIR spectrum of CeO_2 **1** is in good agreement with CeO_2 **2** as shown in Fig 3 (a) [22].

The configuration of the CeO_2 nanoparticles was auxiliary explicated with the help of Raman spectroscopy which is given in Fig. 3 (b). Raman is a common vibrational spectroscopic technique for evaluating molecular motion of materials and thus identifying and analyzing molecular species by providing information regarding the structure and symmetry of the molecule. Raman spectroscopy is based on the detection of inelastic scattering of a monochromatic scattered light. CeO_2 nanoparticles showed a strong intense band at 458 cm^{-1} which agrees to the F_{2g} Raman active-mode of fluorite type cubic structure. Raman spectrum of CeO_2 **1** is in good agreement with CeO_2 **2** as shown in Fig 3 (b) which suggests that CeO_2 **1** has well crystalline fluorite cubic structure [22].

The optical property of synthesized CeO_2 **1** was examined by UV-visible spectrophotometer and result is depicted in Fig. 3 (c). Ultraviolet absorption is a process in which the outer electrons of atoms or molecules absorb radiant energy and undergo transitions to high energy levels. In this process, the spectrum obtained due to optical absorption can be analyzed to get the energy band gap of the material. The optical absorption measurement was carried out at ambient conditions. UV-Vis spectra of the CeO_2 **1** displayed a distinct absorption band at 298 nm like CeO_2 **2** which designates that CeO_2 **1** is optically active and can operate as photo-catalyst which is the assets of any nanomaterial that relay on its optical property. The absorption band of CeO_2 **1** proves that it has fluorite cubic structure like CeO_2 **2** [22]. Moreover, UV spectrum explained no other peak allied with impurity and structural failings which verify that the produced nanoparticles are clean CeO_2. CeO_2 **1** displayed band gap energy (4.16 eV) equal to CeO_2 **2** which calculated according to Eq. (1).

$$E_{bg} = \frac{1240}{\lambda} \text{ (eV)} \qquad (1)$$

Where E_{bg} is the band-gap energy and λ is the wavelength (nm) of the photocatalyst.

3.2. Chemical sensing properties

The CeO_2 **1** nanoparticles were applied for the detection of ethanol in liquid phase by coating on gold electrode with conducting binder. The electrical responses using various concentration of ethanol were measured by two electrodes system that is working electrode and counter electrode. Pd

wire was used as counter electrode while CeO_2 **1** nanoparticles coated gold electrode was used as a working electrode (scheme 1). The black and gray squares in Fig. 4 (a) correspond to the I-V curves of gold electrode with and without CeO_2 **1** nanoparticles. I-V curve of gold electrode without CeO_2 **1** nanoparticles showed slightly high current as compared to I-V curve of gold electrode with CeO_2 **1** nanoparticles. This lower current of CeO_2 **1** nanoparticles coated gold electrode might be due to the surface resistivity caused by CeO_2 **1** nanoparticles covered the surface of the sensor along with conducting binder [28-30].

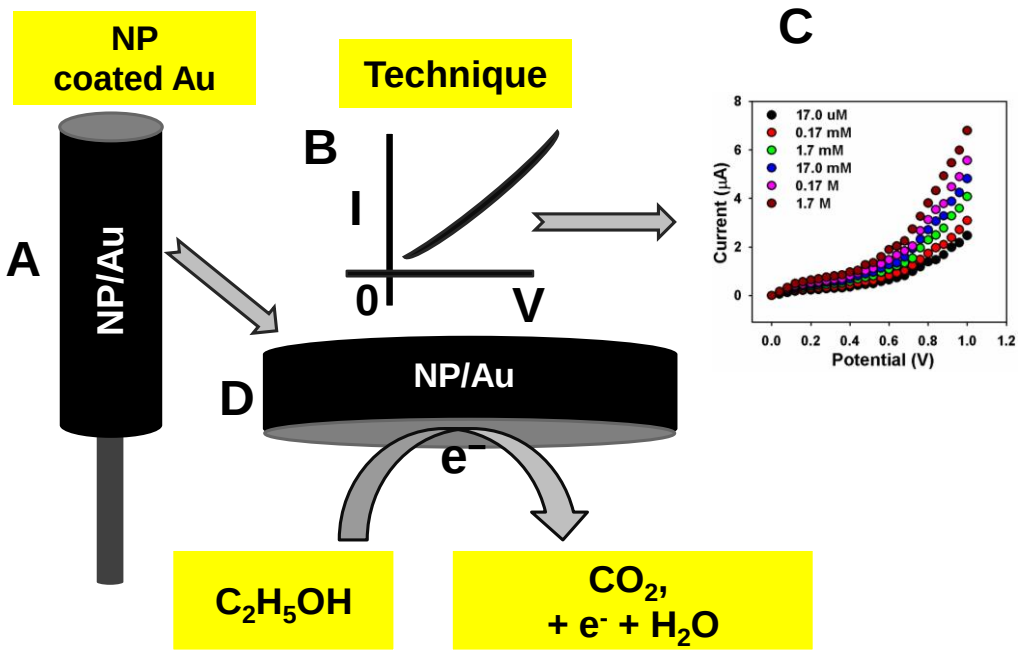

Scheme 1. Schematic views of (a) fabricated AuE with CeO_2 **1** nanoparticles and conducting binders (EC and BCA), (b) I-V detection technique, (c) outcome of I-V experimental result, and (d) reaction occurred at fabricated AuE.

Chemical sensing performance was measured by I-V technique for CeO_2 **1** with various concentrations of ethanol in water at room temperature. Chemical sensing property in the current study obeyed the same trend i.e increase in current with increase of ethanol concentration. The plots of I vs. V were upward curvature, indicating that current (ethanol sensing) increases with increase in voltage. Fig. 4 (b) shows disparity in electrical riposte of the CeO_2 as a role of ethanol. A noteworthy boost in the electrical current was noted by addition of 100.0 μL ethanol (dark square) in 0.1 M phosphate buffer solution (pH = 7.0) as put side by side to electrical response assess in the absence of ethanol (gray square). This happening clearly replicates the sensitivity of CeO_2 nanoparticles in the direction of ethanol sensing functions which may be due to the quick electron switch over and good electro-catalytic oxidation assets of CeO_2 nanomaterials [2-4].

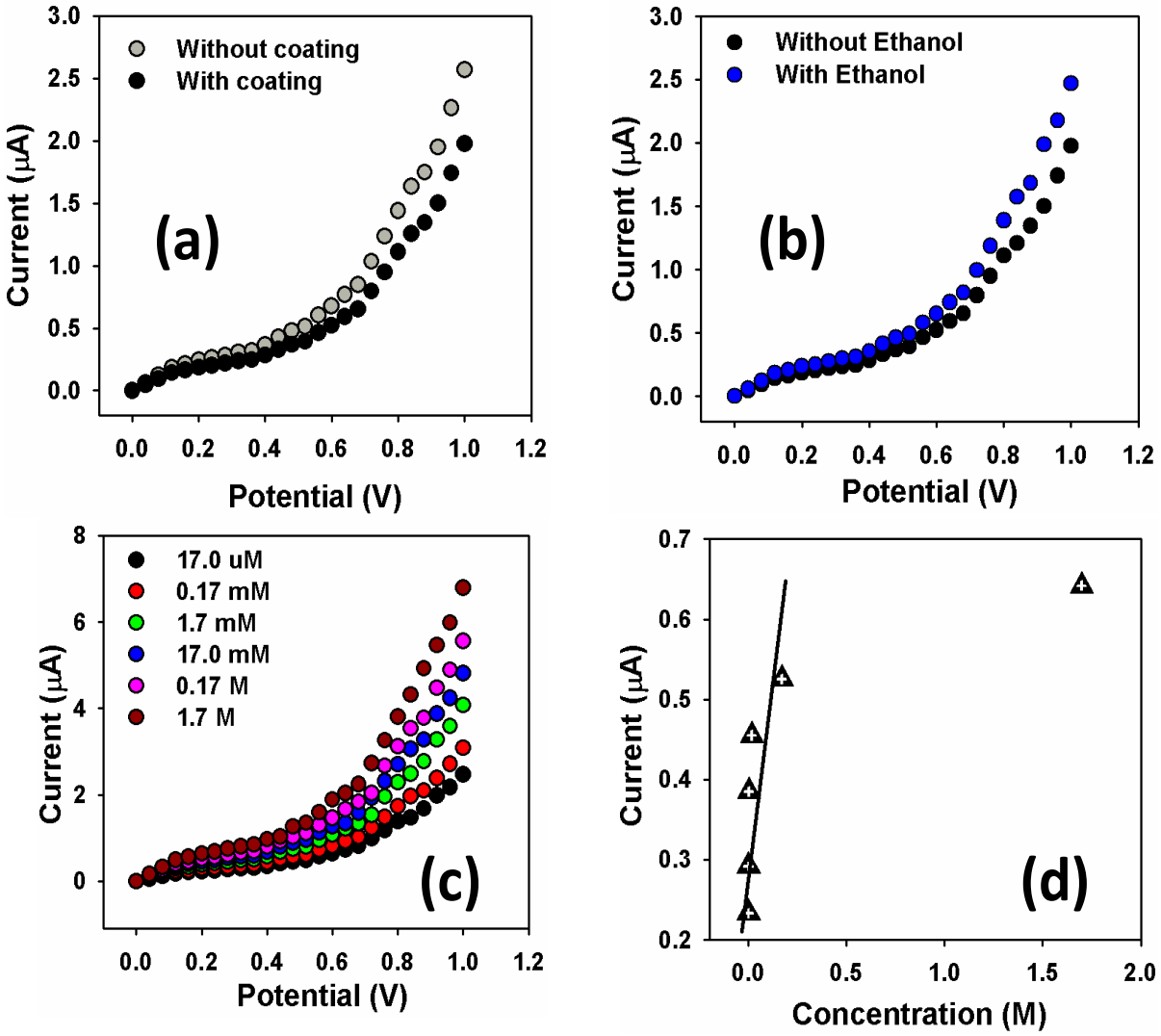

Figure 4. I-V characterization of CeO_2 **1** nanoparticles. (a) Comparison of with and without of CeO_2 **1** nanoparticles coating AuE; b) Comparison of with and without ethanol sample injection; c) Concentration variation of ethanol; and d) calibration plot.

Ethanol experiences two-step procedure by applying to I-V technique and enlarges the conductivity. The first step engage either dehydrogenation or dehydration which creates CH_3CHO (eq. 1) or C_2H_4 (eq. 2) as intermediates, correspondingly.

$$C_2H_5OH \rightarrow CH_3CHO + H_2 \quad (1)$$

$$C_2H_5OH \rightarrow C_2H_4 + H_2O \quad (2)$$

In second step CH_3CHO or C_2H_4 go through oxidation by the nearby oxygen molecules which are physisorbed on the surface spots and creates CO_2, CO, and H_2O (scheme 2).

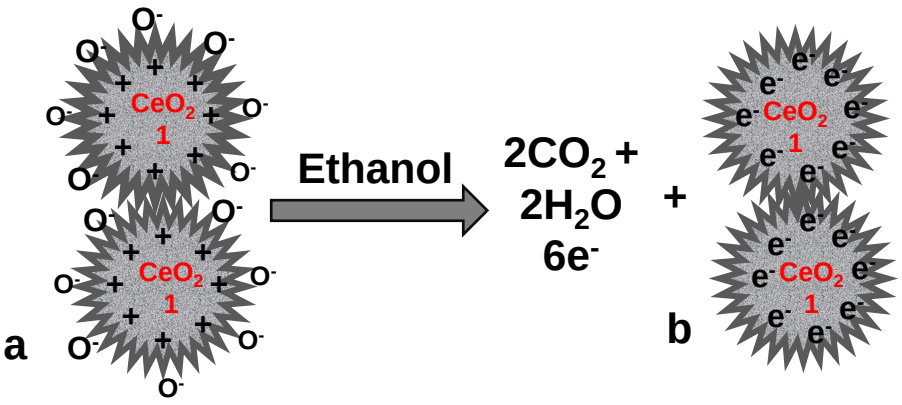

$$CH_3CH_2OH_{(ads)} + 6O^-_{(ads)} \rightarrow 2CO_2 + 3H_2O + 6e^-$$

Scheme 2. Mechanism of ethanol sensing in the presence of CeO_2 **1** nanoparticles.

The cause of C_2H_5OH concentration on the electrical retort (Fig. 4 (c)) of CeO_2 **1** thin film was considered by consecutive addition of C_2H_5OH in the array of 17.0 μM to 1.7 M into 0.1 M PBS solution (pH = 7.0). Fig. 4 (c) explains that electrical current rising with raise in concentration of ethanol which point to the fact that the conductivity of CeO_2 customized electrode was improved with rising the concentration of aimed chemical. This occurrence can be attributed to the raise in ions concentrations during reaction [1,5]. It has generally been understood that a change in the electrical response occurs as the detecting electrolyte becomes more concentrated. The upward curvature I-V plots appear to be consistent with a change in the concentration of electrolyte which we have recently suggested that the increase in current with increase in concentration of detecting chemical for the nanomaterials coated electrodes is due to the sensing effect of nanomaterials. Thus, one might attribute the curved I-V type plots to a change in the chemical sensing. Calibration curve (Fig. 4 (d)) was designed from the difference of target concentration which illustrated two sensitivity areas; region at inferior concentrations (physisorption process) is approximately linear up to 0.2 M with correlation coefficient (R) of 0.9484. The sensitivity is analyzed from the slope of the lesser concentration region of calibration curvature, which is observed to be 1.192 $\mu A.cm^{-2}.M^{-1}$. It is determined from slope of the calibration figure by judging the active surface area of sensors. The linear dynamic array of this sensor displays from 17.0 μM to 0.17 M and the detection limit was guessed ~ 9.7 μM founded on signal to noise ratio (S/N). The superior concentration area (above 0.2 M) illustrates saturation due to chemisorption procedure which possibly can be due to lack of free CeO_2 **1** spots for C_2H_5OH adsorption [9,10].

CeO_2 **1** nanoparticle based ethanol sensor revealed better sensitivity as judge against CeO_2 **2** as shown in Fig. 5 and other reported literature [22,32]. The particle size of CeO_2 **1** is much smaller than

CeO_2 **2**, which has been suggested to be responsible for their higher chemical sensing property. As one can see by comparing the sensitivity, the sensing ability of the CeO_2 increases as the particle size reduces. The sensitivity value for the CeO_2 **1** increases from 0.92 $\mu A.cm^{-2}.M^{-1}$ to 1.192 $\mu A.cm^{-2}.M^{-1}$ as the particle size of the CeO_2 **1** decreases but both nanoparticles showed similar trend of reaction. I-V plots for reactions of CeO_2 **1** and CeO_2 **2** with ethanol are upward curvature. Such type of upward curvature I-V plots have been reported for chemical sensing and suggested as evidence for a change in the electrical response with a change in the concentration of electrolyte [12]. CeO_2 **1** nanoparticles based ethanol sensor also showed higher sensitivity as compared to CuO. Therefore the above upshot without a doubt point to that CeO_2 **1** produced by very easy synthesis process demonstrates noteworthy sensitivity. Therefore CeO_2 **1** can be a beneficial material for the fabrication of sensitive ethanol chemical sensor.

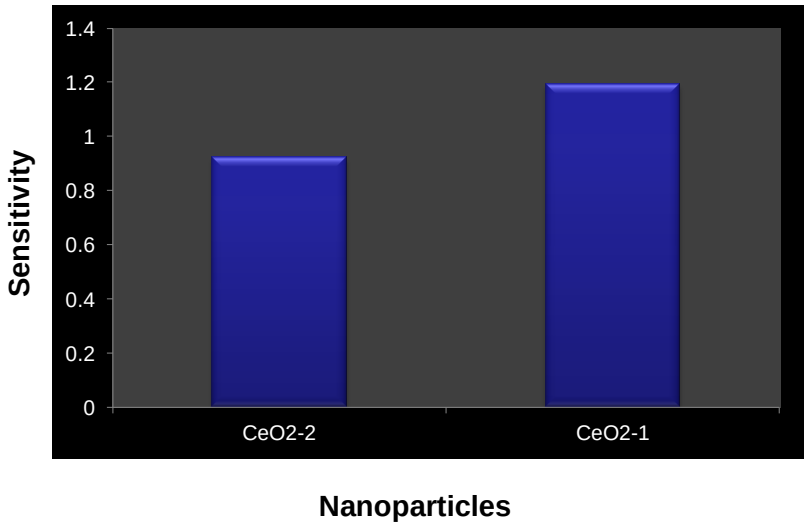

Figure 5. Comparison of ethanol sensing ability (sensitivity) of CeO_2 **1** and CeO_2 **2** nanoparticles.

3.3. Photocatalysis

3.3.1. Photocatalytic performance of CeO_2 1

Aqueous suspension of acridine orange (0.03 mM) was irradiated with a 250 W high pressure mercury lamp in the presence of CeO_2 **1** and lead to alteration in absorbance as a role of irradiation time [16,17,31]. Figure 6 (a) exhibits the amendment in absorption spectra for the photo-catalytic degradation of acridine orange (AO) at dissimilar time periods. It was monitored that irradiation of aqueous suspension of AO dye in the occurrence of CeO_2 **1** guides to decline in absorption intensity. It is observed that the utmost absorbance at 491 nm steadily decreases with the raise in irradiation time.

Figure 6 (b) shows the change in absorbance as a function of irradiation time for the AO in the absence and presence of CeO_2 **1**. Irradiation of an aqueous solution of AO in the presence of synthesized nanomaterial leads to decrease in absorption intensity. Figure 6 (c) demonstrates the design for the % degradation vs irradiation time (min) for the oxygen soaked aqueous suspension of

AO in the existence and nonappearance of the manufactured nanoparticles. The plot describes that 45.8 % of acridine orange is degraded in the occurrence of CeO_2 **1** after 170 minutes of irradiation time while in the nonexistence of nanomaterial no visible loss of dye can be seen.

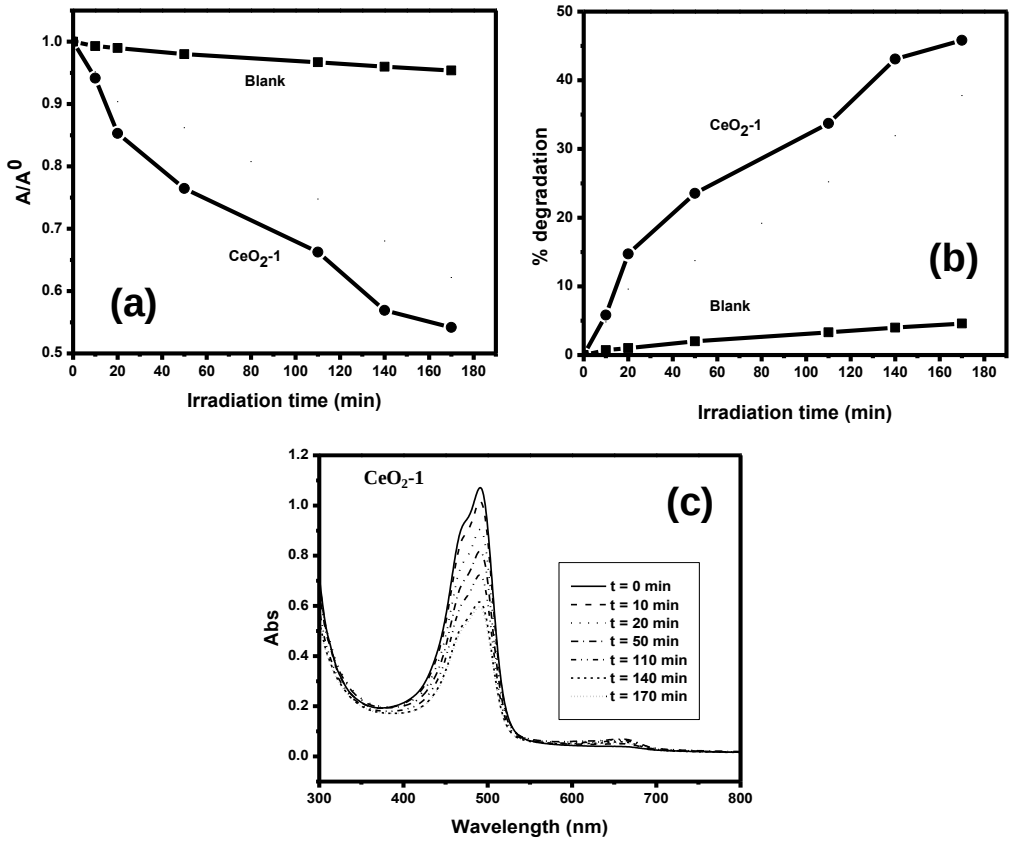

Figure 6. Typical plot for (a) Change in absorbance vs irradiation time for acridine orange, (b) % Degradation vs irradiation time for acridine orange and (c) Change in the absorption spectrum of acridine orange in the presence of CeO_2 **1** nanoparticles.

3.3.2. Reaction kinetics of photo-degradation

In order to realize the degradation behaviors we studied the degradation pattern of AO by Langmuir–Hinshelwood (L–H) model. Langmuir–Hinshelwood (L–H) model well defines the relationship among the rate of degradation and the initial concentration of AO in photo-catalytic reaction [33]. The rate of photo-degradation was calculated by using Eq. (1):

$$r = -dC/dt = K_r K C = K_{app} C \quad \ldots\ldots\ldots\ldots\ldots\ldots \quad (1)$$

Where r is the degradation rate of organic pollutant, K_r is the reaction rate constant, K is the equilibrium constant, C is the reactant concentration. When C is very small, then K_C is negligible; so that Eq. (1) became first order kinetic. Setting Eq. (1) under initial conditions of photo-catalytic procedure, ($t = 0$, $C = C_0$), it became Eq. (2).

$-\ln C/C_0 = kt$……..(2)

Half-life, $t_{1/2}$ (in min) is

$t_{1/2} = 0.693/k$……(3)

Fig. 7 (a) showed that the degradation of AO followed first-order kinetics (plots of $\ln(C/C_0)$ vs time showed linear relationship). First-order rate constants, evaluated from the slopes of the $\ln(C/C_0)$ vs time plots and the half-life of the degraded organic compounds can then be easily calculated by Eq. (3) [33]. The rate constant for CeO_2 **1** and **2** NPs were found to be 0.0035 min^{-1} ($t_{1/2}$ = 198.0 min) and 0.0026 min^{-1} ($t_{1/2}$ = 226.5 min). Thus the kinetic study revealed that CeO_2 **1** is a proficient photo-catalyst for degradation of organic pollutants. Further the degradation rate for the decomposition of AO using CeO_2 **1** and **2** NPs were calculated which were found to be 1.05 x 10^{-4} mole L^{-1} min^{-1} and 7.8 x 10^{-5} mole L^{-1} min^{-1}, respectively.

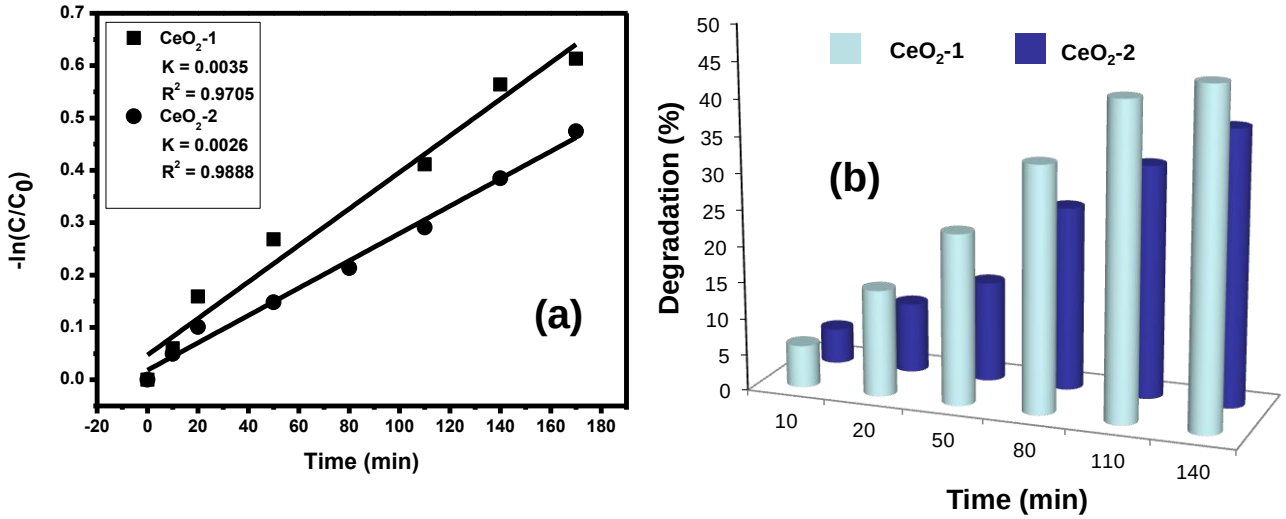

Figure 7. (a) Reaction kinetic and (b) comparison of photo-catalytic activity of CeO_2 **1** with **2.**

3.3.3. Mechanism of photo-degradation

In current study, varied photo-catalysis method is used for the degradation of acridine orange. In brief, when CeO_2 **1** nanoparticles are depicted to light with energy either equal to or bigger than its band gap, development of electron and hole pair occur on surface of CeO_2 **1** nanoparticles. Electron hole pair take part in redox reaction with organic substrate available in water in oxygen presence provided the charge separation is maintained. Hydroxyl radicals ($OH^{\bullet}$) and superoxide radical anions ($O_2^{\bullet -}$) are believed to be the chief vicious agents (oxidizing species) and these oxidative reaction outcomes in the oxidation of the dyes. The whole mechanism of photo-activity of synthesized CeO_2 1 nanoparticles is depicted in scheme 3 [21,22].

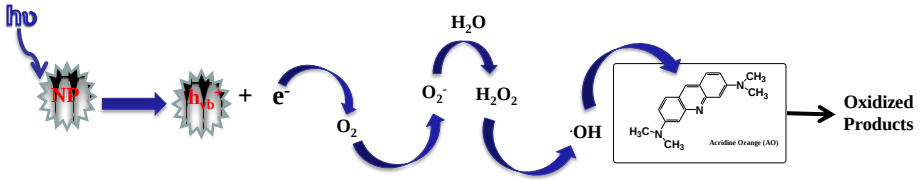

Scheme 3. Mechanism of photodegradation of AO in the presence of CeO_2 **1** nanoparticles.

We compared the photo-catalytic activity of CeO_2 **1** with **2** (Fig. 7b). Both exhibited same trend of degradation but CeO_2 **1** exhibited high photo-catalytic activity as compared to CeO_2 **2**. It has been observed that CeO_2 **1** and **2** shows different photo-catalytic activities to AO under same condition as shown in Fig. 7 (b). The particle size of CeO_2 **1** is much smaller than CeO_2 **2**, which has been suggested to be responsible for their higher photo-catalytic activity. Thus the mentioned results clearly signify that CeO_2 manufactured by extremely simple synthesis method displays significant photo-catalytic activity. That makes it a useful photo-catalyst alongside other metal oxide.

4. CONCLUSION

A sensitive chemical sensor for recognition of ethanol and active photo-catalyst for degradation of acridine orange has been developed using CeO_2 **1** nanoparticles which were newly produced at low-temperature in great quantity using uncomplicated hydrothermal process in the presence of urea. This sensor and photo-catalyst is applicable for the detection of hazardous chemical [10] such as ethanol in micro level and degradation of organic pollutant [21] such as acridine orange in aqueous media. The sensitivity of the sensor and activity of the photo-catalyst are reasonably high as compared to the literature [12]. The formulated ethanol sensor founded on CeO_2 **1** nanoparticles demonstrated better sensitivity, lower finding limit with linearity in small response time. Initially the calibration curve is linear which suggests that physisorption process takes place due to free available space for adsorption of ethanol and later at higher concentration, chemisorption process takes place due to lack of free CeO_2 **1** spots for C_2H_5OH adsorption [9,10]. Further by comparing the performance of CeO_2 **1** with **2**, it was found that CeO_2 **1** nanoparticles have high sensitivity and photo-catalytic activity which is concluded that the lower particle size of CeO_2 **1** responsible for their higher sensitivity and photo-catalytic activity [22]. Significantly, this contribution will lead to considerable improvement in the field of chemical sensor and photo-ctalysis and will contribute to the environmental monitoring.

ACKNOWLEDGEMENT
We would like to thank the Deanship of Scientific Research at King Abdulaziz University for the support of this research *via* a Research Group Track Grant (**No. 3-102/428**). Center of Excellence for Advanced Materials Research, King Abdulaziz University is also highly acknowledged.

References

1. S.B. Khan, M.M. Rahman, E.S. Jang, K. Akhtar, H. Han, *Talanta* 84 (2011) 1005–1010.
2. M.M. Rahman, S.B. Khan, A. Jamal, M. Faisal, A.M. Asiri, *Talanta* doi.org/10.1016/j.talanta.2012.03.027.
3. M.M. Rahman, A. Jamal, S.B. Khan, M. Faisal, *Superlat. Microstruc*. 50 (2011) 369-376.
4. S.B. Khan, M. Faisal, M.M. Rahman, A. Jamal, *Talanta* 85 (2011) 943-949.
5. M. Faisal, S.B. Khan, M.M. Rahman, A. Jamal, *Appl. Surf. Sci.* 258 (2011) 672-677.
6. R.K. Jain, M. Kapur, S. Labana, B. Lal, P.M. Sharma, D. Bhattacharya, I.S. Thakur, *Curr. Sci*. 89 (2005) 101–112.
7. S.E. Stanca, I.C. Popescu, L. Oniciu, *Talanta* 61 (2003) 501–507.
8. G.X. Zheng, J.M. Song, Y.H. Wang, S.P. Yu, X.G. Li, *Huan Jing Ke Xue* 30 (2009) 1306-1314.
9. M. Faisal, S.B. Khan, M.M. Rahman, A. Jamal, *J. Mater. Sci. Technol*. 27 (2011) 594-600.
10. M.M. Rahman, A. Jamal, S.B. Khan, M. Faisal, *Biosens. Bioelectron*. 28 (2011) 127-134.
11. R.M. Banik, Mayank, Rajiv Prakash, S.N. Upadhyay, *Sens. Actuat*. B 131 (2008) 295–300.
12. M. Faisal, S.B. Khan, M.M. Rahman, A. Jamal, A. Umar, *Mater. Lett.* 65 (2011), 1400–1403.
13. S.C. Bondy, S.X. Guo, *Europ. J. Pharmacol*. 270 (1994) 349-355.
14. C. Lindi, G. Montorfano, P. Marciani, *Alcohol* 16 (1998) 311-316.
15. M.M. Rahman, A. Jamal, S.B. Khan, M. Faisal, *J. Nanoparticle Res*. 13 (2011) 3789-3799.
16. A. Jamal, M.M. Rahman, M. Faisal, S.B. Khan, *Mater. Sci. Applicat*. 2 (2011) 676-683.
17. M. Faisal, S.B. Khan, M.M. Rahman, A. Jamal, M.M. Abdullah, *Appl. Surf. Sci*. doi.org/10.1016/j.apsusc.2012.04.075.
18. M.M. Rahman, A. Jamal, S.B. Khan, M. Faisal, *J. Phys. Chem*. C 115 (2011) 9503–9510.
19. M.M. Rahman, A. Jamal, S.B. Khan, M. Faisal, *ACS Appl. Mater. Interfaces* 3 (2011) 1346–1351.
20. M.M. Rahman, S.B. Khan, A. Jamal, M. Faisal, A.M. Asiri, *Sens. Transduc. J.* 134 (2011) 32-44.
21. M. Faisal, S.B. Khan, M.M. Rahman, A. Jamal, *Chem. Engineer. J.* 173 (2011) 178-184.
22. S.B. Khan, M. Faisal, M.M. Rahman, A. Jamal, *Sci. Tot. Environ*. 409 (2011) 2987–2992.
23. F. Niu, D. Zhang, L. Shi, X. He, H. Li, H. Mai, T. Yan, *Mater. Lett*. 63 (2009) 2132-2135.
24. M. Palard, J. Balencie, A. Maguer, J.F. Hochepied, *Mater. Chem. Phys*. 20 (2010) 79-88.
25. F. Meshkani, M. Rezaei, *Powder Technology*, 199 (2010) 144-148.
26. O. Tunusoglu, R.M. Espi, U. Akbey, M.M. Demir, *Colloids and Surfaces A: Physicochemical and Engineering Aspects*, 395 (2012) 10–17.
27. T. Sreethawong, S. Ngamsinlapasathian, S. Yoshikawa, *Materials Letters*, 78 (2012) 135–138
28. S.G. Ansari, Z.A. Ansari, H.K. Seo, G.S. Kim, Y.S. Kim, G. Khang, A. H.S. Shin, *Sens. Actuators* B 132 (2008) 265-71.
29. S.G. Ansari, Z.A. Ansari, R. Wahab, Y.S. Kim, G. Khang, A. H.S. Shin, *Biosens Bioelectron*. 23 (2008) 1838-1842.
30. S.G. Ansari, R. Wahab, Z.A. Ansari, Y.S. Kim, G. Khang, A. Al-Hajry, H.S. Shin, *Sens. Actuators* B 137 (2009) 566-573.
31. M. Faisal, M.A. Tariq, M. Muneer, *Advanc. Sci. Lett*. 3 (2010) 512–517.
32. C.K. Liu, J.M. Wu, H.C.Shih, *Sens. Actuators* B 150 (2010) 641-648.
33. K.M. Parida, L. Mohapatra, *Chem. Engineer. J.* 173 (2011) 178-184.